**ARTICLE TYPE**

# A TiS₂ nanosheet enhanced fluorescence polarization biosensor for ultra-sensitive detection of biomolecules

Xiang Li,[a] Xuelian Ding,[b] Yongfang Li,[c] Linsong Wang[c] and Jing Fan*[a]

**Development of new strategies for the sensitive and selective detection of ultra-low concentration of specific cancer markers is of great importance for assessing cancer therapeutics due to its crucial role in early clinical diagnoses** 10 **and biomedical application. In this work, we have developed two types of fluorescence polarization (FP) amplification assay strategies for the detection of biomolecules by using TiS₂ as a FP enhancer and Zn²⁺-dependent self-hydrolyzing deoxyribozymes as catalysts to realize enzyme-catalyzed** 15 **target-recycling signal amplification. One approach is based on terminal protection of small-molecule-linked DNA, in which biomolecular binding to small molecules in DNA-small-molecule chimeras can protect the conjugated DNA from degradation by exonuclease I (Exo I); the other approach is** 20 **based on terminal protection of biomolecular bound aptamer DNA, in which biomolecules directly bound to the signal strand aptamer DNA can protect the ssDNA from degradation by Exo I. We select folate receptor (FR) and thrombin (Tb) as model analytes to verify the current** 25 **concept. It is shown that under optimized conditions, our strategies exhibit high sensitivity and selectivity for the quantification of FR and Tb with low detection limits (0.003 ng/mL and 0.01 pM, respectively). Additionally, this strategy is a simple "mix and detect" approach, and does not require** 30 **any separation steps. This biosensor is also utilized in the analysis of real biological samples, the results compare well with those obtained by enzyme-linked immunosorbent assay (ELISA).**

35 ## Introduction

The detection and quantification of biomolecules is of great significance in molecular diagnostics, biomedical research and clinical diagnoses.[1] At present, conventional methods, such as 40 high performance liquid chromatography and enzyme-linked immunosorbent assay (ELISA) have been widely used in the detection of biomolecules. However, these methods usually need costly apparatus and complicated pretreatment procedures such as enzyme immobilization, separation, and washing steps. Thus, 45 seeking for simple and homogeneous assay approaches to accurately detect trace amounts of such biomolecules is the development trends in recent years.

It has been reported that when some particular biomolecules are bound to the terminal of single strand DNA (ssDNA), ssDNA 50 can avoid hydrolysis by Exonuclease (such as Exo I or Exo III).[2] This phenomenon is called terminal protection of single strand DNA. According to the principle of terminal protection, single-strand DNA probes have been popularly employed in the development of novel methods for the detection of biomolecules 55 by using various signal-transduction approaches such as electrochemistry, colorimetry, fluorescence, and so on.[2b-e,3] Due to its simplicity, rapidness and versatility, fluorescence polarization (FP) assay has attracted more and more interests. Indeed, traditional FP assays have been widely used for routine 60 analysis of various biomolecules.[4] While these strategies have their distinct advantages, there remain some challenging problems such as low sensitivity. In order to improve the detection sensitivity, different amplification methods have been developed for FP detection. Of these methods, the mass 65 amplification strategy has been utilized to increase the sensitivity of FP assays in a series of recent studies. For example, proteins, gold nanoparticles (AuNPs), single-walled carbon nanotubes (SWNTs) and graphene oxide (GO) have been used as "FP enhancers" for mass amplification FP assay of small organic 70 molecules, proteins, and metal ions.[5] Although enhanced sensitivity is demonstrated by these amplification strategies, it is still strictly limited owing to the 1:1 binding ratio, which means that one probe can bind with only one target molecule.

Recently, the strategies based on enzyme-catalyzed target 75 recycling signal amplification have demonstrated great potential for increasing the sensitivity of sensor assays.[6] Toward this end, nuclease (such as endonuclease, exonuclease and nicking enzyme) has been employed as biocatalyst in the target recycling-oriented amplification assays for sensitive detection of 80 biomolecules.[7] Despite their high sensitivity, it is still necessary to develop new class of biocatalysts in the sensing systems. In recent years, deoxyribozymes (DNAzymes) have attracted considerable attention due to their excellent capability in mediating signal amplification.[8] Depending on specific metal ions 85 or neutral molecules used as cofactors, these DNAzymes (nucleic acids) show high protein enzyme-like catalytic hydrolytic cleavage activities toward certain substrates. In particular, Zn²⁺ and Pb²⁺ dependent RNA-cleaving DNAzymes (named 8-17E DNAzyme) have been extensively employed for amplification

detection of a variety of targets.[9] However, these systems have some limitations such as the use of unstable molecules (RNA) as the substrate strand. Recently, Breaker's group[10] reported a $Zn^{2+}$-dependent DNA-self-hydrolyzing deoxyribozymes, which can selectively and rapidly hydrolyze their DNA substrates at a sequence-specific site in the presence of $Zn^{2+}$. This unique advantage makes the self-hydrolyzing deoxyribozymes as ideal biocatalysts for amplified sensing applications. Unfortunately, compared with RNA-cleaving DNAzymes, such DNA-self-hydrolyzing deoxyribozymes have not been reported in any attempts for their use in the biosensor application.

As two-dimensional (2D) graphene analogues, 2D transition metal dichalcogenide nanosheets (TMD NSs) with single- and few-layeres, such as $MoS_2$, $WS_2$, $TaS_2$ and $TaNbS_2$, have received considerable attention from all over the world in recent years. Due to their unique optical, electronic and electrochemical properties, TMD NSs exhibit many promising applications in the fields of electronics, sensors, optics, catalysis, and energy storage.[11] Like graphene nanomaterials, TMD NSs are known to efficiently quench the fluorescence of organic dyes through long-rang nanoscale energy transfer. Therefore, TMD NSs are very promising for the development of biosensors for detection of various biomolecules because of their unique characteristics such as large-scale production and good dispersion in aqueous solution. For example, $TiS_2$ nanosheet has been reported to exhibit the capability for discriminating single-stranded DNA (ssDNA) and double stranded DNA (dsDNA), which offers an opportunity to develop the applications of $TiS_2$ nanosheets in biosensors areas.[12] However, exploration of the $TiS_2$ nanosheet in the biosensors still remains at a very early stage.

Herein, we have developed a fluorescence polarization amplification assay strategy for the detection of biomolecules by using $TiS_2$ as a FP enhancer and $Zn^{2+}$-dependent self-hydrolyzing deoxyribozymes as catalysts to realize enzyme-catalyzed target recycling signal amplification. Compared with traditional homogeneous aptasensors, our strategy provides several significant advantages. First, by using the $Zn^{2+}$-dependent DNA-self-hydrolyzing deoxyribozymes coupled with $TiS_2$ enhancement approach, the detection sensitivity can be significantly improved by three orders of magnitude over traditional assays and fluorescence resonance energy transfer (FRET) methods. Second, the proposed sensing assays can be conducted in aqueous solution, and not requiring separation and other troublesome procedures. More importantly, the $Zn^{2+}$-dependent DNA-self-hydrolyzing deoxyribozymes are used, for the first time, for the detection of biomolecules, thus significantly broadening the scope of $Zn^{2+}$-dependent self-hydrolyzing deoxyribozymes in biochemical and biomedical studies. From these advantages, we expect that this strategy may become a generalized platform for biomolecules detection.

## Materials and methods

### Reagents and materials

All oligonucleotides used in this work were synthesized and HPLC purified by Shanghai Sangon Biotechnology Co., Ltd. (Shanghai, China). The sequences of all oligonucleotides (probe 1, probe 2 and probe 3) were listed in Table S1. Folate receptor (FR), thrombin (Tb), human serum albumin (HSA), immunoglobulin G (IgG), immunoglobulin E (IgE), strepavidin (SA) and adenosine triphosphate (ATP) were purchased from Shanghai Sangon Biotech. Co., Ltd. (Shanghai, China). Exo I and $10 \times$ reaction buffer (670 mM glycine-KOH, 67 mM $MgCl_2$ and 10 mM dithiothreitol, pH 9.5) were obtained from New England Bio Labs Ltd. (Beijing, China). The DNAzyme reaction buffer contains 10 mM Tris-buffer (pH 7.0), 20 mM $MgCl_2$ and $ZnCl_2$. Titanium sulfide powder (200 mesh, 99.9%) was commercially available from Sigma-aldrich (China). All other reagents were analytical grade and used without further purification. Doubly distilled water was used throughout the work. All stock solutions were stored in the dark at 0-4℃.

### Apparatus

Fluorescence polarization was measured with a Cary Eclipse fluorescence spectrophotometer equipped with a polarization filter (Varian, America). The excitation and emission wavelengths were set at 495 nm and 520 nm, respectively, for FP assay. The fluorescence polarization measurements were carried out by using a single cell peltier accessory to control temperature. Transmission electron microscopy (TEM) images were record on a JEM 2100 microscope (JEOL, Japan). Atomic force microscopy (AFM) images were recorded on a PicoScan atomic force micro-scope (USA) at ambient temperature. Raman spectra were recorded on a Raman micro-spectrometer (Renishaw, UK) at ambient temperature.

### Synthesis of the Layered $TiS_2$ Nanosheet

$TiS_2$ nanosheet was synthesized from bulk $TiS_2$ by sonication-assisted liquid exfoliation according to previously reported protocol with slight modification.[13] In a typical procedure, $TiS_2$ powder (150 mg) was added into a three-neck round-bottom flask and protected with argon gas. Then 10 mL of n-BuLi in hexane (15.0 mmol) was introduced into the flask by a syringe. After that, the mixture was sonicated for 2 h at 40 ℃ to obtain Li-intercalated $TiS_2$. The resultant dispersion was left to stand for overnight and the supernatant containing the residual n-BuLi was removed. The precipitate was washed with cyclohexane and anhydrous ethanol for several times, and then vacuum dried at room temperature overnight for the next experimental procedures. Under $N_2$ atmosphere, the deaerated ultrapure water (20 mL) was carefully added into a tube containing 20 mg of Li-intercalated $TiS_2$. The aqueous suspension of Li-intercalated $TiS_2$ was immersed into ice water and ultrasonicated for 2 h. Then, the dark dispersion was centrifuged at 5000 rpm for 10 min to remove the unexfoliated flakes. The supernatant was collected by centrifugation at 15 000 rpm for 20 min and further washed with water. The as-obtained black precipitate was dispersed in water for further characterizations and applications.

### Assay Procedures

In a typical experiment, different concentrations of FR were incubated in dark for 50 min at 37℃ in 480 μL of Tris-buffer

containing 50 nM probe 1 to allow complete interaction between FR and folate-ssDNA. Then, 150 U of exonuclease I in 5 μL 10 × exonuclease I reaction buffer was added to the mixture in order to degrade the unbound probes and the resultant mixture was incubated for 30 min at 37℃, followed by heating at 80℃ for 15 min to inactivate the exonuclease I. After this step, 10 μL 2 μM probe 2 was added, and the mixture was incubated at 37℃ for 30 min. Then 5 μL of $TiS_2$ nanosheet was added to the mixture and the fluorescence polarization measurements were carried out after 5 min of the $TiS_2$ nanosheet addition. The procedure for Tb measurements was the same as that of FR detection described above.

### Preparation of the real biological samples

For the determination of FR in real biological samples, the serum samples from three advanced ovarian cancer patients and three healthy women (obtained from Sanquan Medical College, Xinxiang Medical University) were prepared. Briefly, the venous blood samples were collected and naturally solidified at 4℃ in fridge overnight. Then the mixture was centrifuged at 3000 rpm for 5 min at 4℃ and the upper supernatant solution was collected for further detection. For our proposed signal amplified fluorescence polarization strategy, the collected samples were diluted 50-fold with Tris-buffer and then immediately used for FR detection. The detection process of FR in real biological sample was the same as in the buffer solution.

For the Tb detection in human blood samples, three healthy normal human plasma samples (provided by Sanquan Medical College, Xinxiang Medical University) were collected in the citrate anticoagulated tubes. The pretreatment of blood samples were made according to the method reported in the literatures.[7c,14] Briefly, 0.1 mL of human plasma was quickly mixed with 1.25 mL of ammonium sulfate (2 M) and 1 mL of NaCl (0.1 M). After 4 min incubation, the mixture was centrifuged and the upper supernatant solution was collected. Then, $CaCl_2$ (0.03 M) with 8 nM human factor Xa was then added to the plasma to promote the transformation from prothrombin to thrombin. Finally, the resulting plasma was diluted 100-fold with Tris-buffer, and immediately used for Tb detection. The detection process of Tb in human blood sample was the same as in the buffer solution.

## Results and discussion

The as-prepared $TiS_2$ nanosheets were characterized by transmission electron microscopy (TEM) and atomic force microscopy (AFM). As shown in Fig. 1a-b, TEM images of the dispersed $TiS_2$ in solution revealed that the morphology was a two-dimensional thin-layer nanosheet. The high-resolution TEM image and the selected area electron diffraction (SAED) (shown in Fig. 1c) indicate that $TiS_2$ nanosheet had an interplanar distance of 3.0 Å, which matches well with the (100) plane.[13] To examine the thickness of the prepared $TiS_2$ nanosheets, AFM meseasurement was also carried out. As shown in Fig. 1d, the thickness of the nanosheets was around 1.0 nm, which evidences the successful synthesis of the single-layer $TiS_2$ nanosheets. In Fig. S1a, the two Raman peaks corresponding to the high energy $A_{1g}$ mode (332 cm$^{-1}$) and lower energy $E_{1g}$ mode (229 cm$^{-1}$),

respectively, maped exactly onto a reported spectrum of $TiS_2$.[13a] As shown in Fig. S1b, zeta potential of the as-prepared $TiS_2$ in aqueous solution was also measured to explain its excellent aqueous stability. The dispersed $TiS_2$ was negatively charged, with a zeta potential of -20.7 ± 0.7 mV. The high surface charge induced high electrostatic repulsion between $TiS_2$ nanosheets, which kept them stable in the aqueous dispersion. The UV-vis absorption spectrum of the $TiS_2$ dispersions was also determined (shown in Fig. S2). It can be seen that the light absorption covered a wide range of wavelength from UV to visible region, suggesting that the material could be an ideal energy acceptor for diverse chromophores. In addition, because the fluorescence polarization value (FP) is defined as the ratio of fluorescence intensities parallel and perpendicular with respect to plane-polarized excitation light, FP values depend mainly upon their molecular volume (molecular weight) at constant temperature and solution viscosity.[4d, 4e] When $TiS_2$ nanosheet was used as "FP enhancer", the strong absorption of $TiS_2$ nanosheet did not affect the fluorescence polarization signal. Similar results were reported for the use of other nanomaterials (such as Au NPs, CNTs, graphene oxide, $WS_2$ and so on) as "FP enhancer" for mass amplification FP assay.
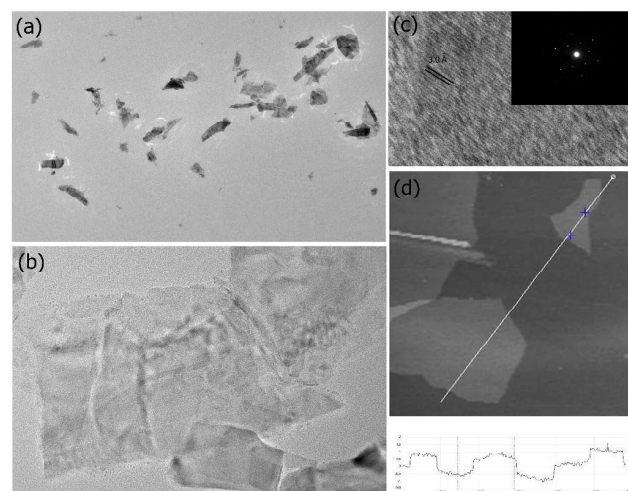


**Fig. 1** Characterization of the as-prepared $TiS_2$ nanosheets. (a and b), TEM images of the prepared nanomaterials; (c), high-resolution TEM image of the typical $TiS_2$ nanosheets; Inset, the corresponding SAED pattern of $TiS_2$ nanosheets with the electron beam perpendicular to its basal plane; (d), AFM height image of the single-layer $TiS_2$ nanosheets.

Similar with other two-dimensional (2D) graphene analogues, $TiS_2$ nanosheets can adsorb dye-labeled single-stranded DNA (ssDNA) via van der Waals interaction between nucleobases and the basal plane of nanosheets.[12] it is also expected that $TiS_2$ nanosheets can exhibit different affinity toward single-stranded DNA with different lengths of bases. To verify this hypothesis, we investigated the fluorescence quenching ratio of $TiS_2$ nanosheets to ssDNA with different lengths because the fluorescence quenching ratio is directly proportional to the amount of DNA adsorbed.[11e-f] As shown in Fig. S3, the fluorescence quenching ratio of $TiS_2$ nanosheets to ssDNA increased with increasing base number of ssDNA. When the

concentrations of oligonucleotide and TiS$_2$ nanosheet were fixed, it was found that the fluorescence quenching ratio of TiS$_2$ to FAM-labeled ssDNA containing 19 bases (named 19-F) was 98%. In contrast, for the similar ssDNA containing 6 bases (named 6-F), only 35% fluorescence quenching ratio was obtained. This result indicates that the affinity of the short ssDNA to TiS$_2$ was significantly weaker than that of the long ssDNA, which forms the basis for the design of the TiS$_2$ nanosheet based fluorescence polarization assay for biomolecules detection.

Based on the terminal protection of small-molecule-linked DNA, we developed a novel fluorescence polarization amplification approach for the detection of biomolecules by using folate receptor (FR)-folate system as a model. FR is a highly selective biomarker over-expressed by many primary and metastatic types of cancer.[15] Therefore, quantitative analysis of FR is especially important in early cancer diagnosis. Zn$^{2+}$-dependent self-hydrolyzing deoxyribozymes (DNAzymes) containing an enzyme strand and a substrate strand was employed in this strategy to selectively cleave the substrate DNA at a sequence-specific site in the presence of Zn$^{2+}$ (Scheme S1).[16]
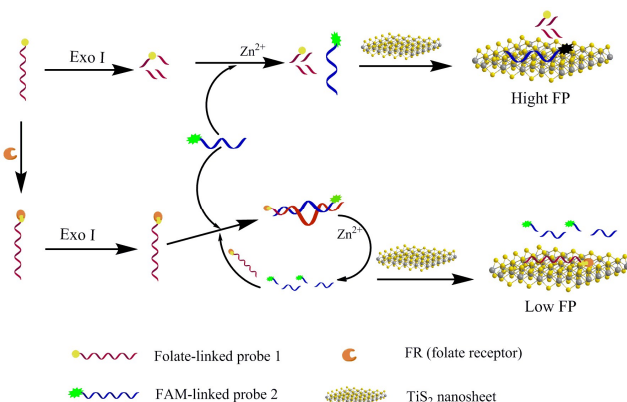


**Scheme 1.** The working principle of TiS$_2$ nanosheet enhanced fluorescence polarization biosensor for FR detection via terminal protection of small-linked DNA and DNAzyme assisted signal amplification.

The working principle of our detection strategy was schematically represented in Scheme 1. The enzyme strand is linked with a folate at its 3' end, and the substrate strand is labeled with a carboxy fluorescein (FAM) at its 3' end. In the absence of FR, the folate-linked enzyme strand (probe 1) is hydrolyzed into mononucleotides by Exo I from the 3' to 5' direction. As a result, DNAzymes can not be formed due to the lacking of enzyme strands. The introduction of TiS$_2$ into the solution of FAM-labeled substrate strand (probe 2) may result in strong binding between nucleotide bases and basal plane of TiS$_2$ nanosheet via van der Waals interactions. This brings the fluorophore into close proximity with the TiS$_2$ surface, thus the FAM dye exhibits very high FP value due to the extraordinarily large volume of TiS$_2$ nanosheet with slow rotation. However, in the presence of a FR, the FR protein can specifically bind to the folate capped at the 3'-end of probe 1 with strong affinity. The protein tethered at the 3'-end in a 1:1 ratio can protect probe 1 from the hydrolysis by Exo I because of the significant steric-hindrance. In this case, probe 1 and probe 2 can hybridize with

each other to form a DNAzyme structure. Upon incubation with Zn$^{2+}$, the DNAzyme is activated and the FAM-labeled probe 2 (the substrate strand) is cleaved at the specific site into two short DNA fragments (one contains 6 bases, the other contains 13 bases). The cleaved short FAM-labeled DNA fragment is kept away from TiS$_2$ nanosheet surface due to the weak affinity of the short oligonuleotide fragment to TiS$_2$, thus the FAM dye exhibits a low FP value with fast rotation. In addition, the probe 1 released from Zn$^{2+}$-assisted cleavage of DNAzyme can hybridize with another FAM-labeled probe (probe 2) to initiate the second cycle. Once the DNAzyme cleavage process is triggered, continuous cleavage of the FAM-labeled probe (probe 2) would take place. Finally, each target can go through many cycles, leading to a substantial decrease of the FP value and thus signal amplification.
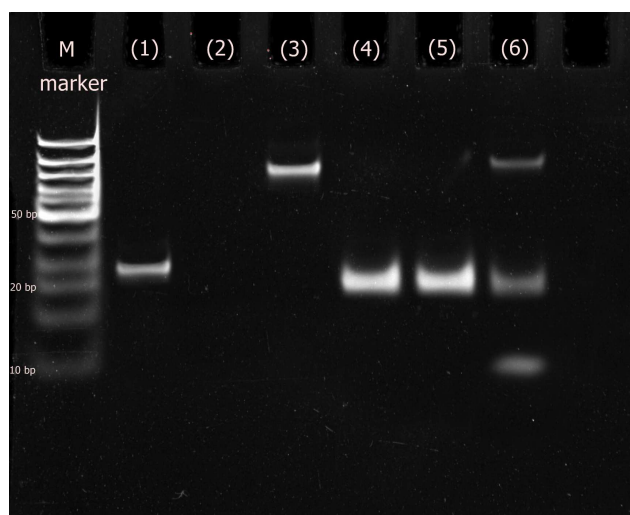


**Fig. 2** Native PAGE analysis of the sensing system. Lane M, DNA size marker; Lane 1, probe 1 alone; lane 2, probe 1 + Exo I; lane 3, probe1 + FR+ Exo I; lane 4, probe 1 + Exo I + probe 2; lane 5, probe 1 + Exo I + probe 2 + Zn$^{2+}$; lane 6, probe 1 + FR+ Exo I+ probe 2 + Zn$^{2+}$. All samples were monitored by using non-denaturing 15% polyacrylamide gel electrophoresis in 1 × TBE at 70 V for 80 min. The gel was recorded by the Tanon GIS-1000 Gel Imaging System after being stained by ethidium bromide.

To confirm the feasibility of the present strategy, native polyacrylamide gel electrophoresis was performed to validate the experimental results. As shown in Fig. 2, a bright band on lane 1 was observed when probe 1 was not subjected to Exo I treatment. However, after incubating with Exo I, no bright band was found in lane 2. This result confirms that the folate-linked single-stranded probe 1 was hydrolyzed into mononucleotides by Exo I, and the mononucleotides could migrate out of the gel. When probe 1 was firstly incubated with FR and followed by Exo I treatment, a bright band was still observed on lane 3. This suggests that the protection of probe 1 from Exo I-mediated digestion was aroused from specific binding of FR to the folate-linked DNA. In the case of no FR in the probe 1/probe 2 system, the probe 1 was firstly incubated with Exo I and then hybridized with probe 2, no new product band was obtained regardless of the absence or presence of Zn$^{2+}$ (see lanes 4 and 5), which suggests that probe 1 was hydrolyzed into mononucleotides by Exo I and

could not hybridize with probe 2 to form DNAzyme structure. However, a new product band (cleaved probe 2) appeared in lane 6 only in the presence of FR. This demonstrates that FR could specifically bind to the FA linked probe 1 to avoid the hydrolysis
5 of probe 1 by Exo I. The residual probe 1 could hybridize with probe 2 to form an active $Zn^{2+}$-dependent DNAzyme structure, and then $Zn^{2+}$ activated the DNAzyme self-hydrolyzing generating short DNA fragments. These results are in agreement with those shown in scheme 1, demonstrating the feasibility of
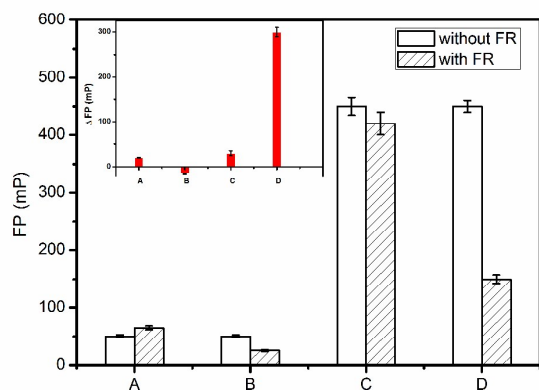10 our sensing protocol.



**Fig. 3** FP values at different sensing systems in the absence and presence of FR: (A), probe 1 + probe 2; (B), probe 1+ probe 2 + $Zn^{2+}$; (C), probe 1+ probe 2 + $TiS_2$; (D), probe 1 + probe 2+ $TiS_2$
15 + $Zn^{2+}$. Inset is the $\Delta FP$ values of the above systems generated by 5 ng/mL of FR ($\Delta FP = FP_0$-FP, where $FP_0$ and $FP$ are the $FP$ values in the absence and presence of FR, respectively). [probe 1] = 48 nM, [probe 2] = 40 nM, $[TiS_2]$ = 25 µg/mL, [FR] = 5 ng/mL, $[Zn^{2+}]$ = 2 mM and [Exo I] = 10 U.

20

The changes in the target-induced FP value under different conditions were also investigated to verify the feasibility of the designed amplification strategy for FR detection. As shown in Fig. 3, in the probe 1/probe 2 system, FP value of the FAM-labeled
25 probe 2 was 50 in the absence of FR, but it was increased to 70 upon addition of FR into the probe 1/probe 2 systems. When $Zn^{2+}$ was introduced into the probe 1/probe 2 system, the FP value was decreased to 35 in the presence of FR. This indicates that $Zn^{2+}$ could activate the DNAzyme and then catalyze the cleavage of
30 FAM-labeled probe 2 to generate short FAM-DNA fragments (6 bases) with fast rotation. When $TiS_2$ nanosheet and $Zn^{2+}$ were introduced into the system, the FP value of probe 2 was obviously increased to 450 in the absence of FR, which was about 9-fold higher than that without $TiS_2$. This suggests that FAM-labeled
35 probe 2 was strongly adsorbed on $TiS_2$ surface, leading to the increase in the molecular volume of the FAM-labeled probe 2 /$TiS_2$ complexes. Meanwhile, upon addition of FR, the FP value of this system was significantly decreased to 150. The $\Delta FP$ ($\Delta FP$ = $FP_0$-FP) value of this system was approximately 10 times
40 higher than that of the probe 1/probe 2/ $TiS_2$ system (only using $TiS_2$ enhancement) and 20 times higher than that of the probe 1/probe 2/ $Zn^{2+}$ system (only using $Zn^{2+}$ assisted target-recycling signal amplification), where $FP_0$ and FP are the FP values in the absence and presence of FR, respectively. As DNAzyme cleavage
45 would result in a large amount of DNA fragments, such DNA

fragments would induce the incomplete adsorption on the surface of $TiS_2$ nanosheets. In order to verify whether the low fluorescence polarization value may be caused by incomplete adsorption of the fragments, additional control experiments were
50 performed (detail results were shown in Fig. S4). The experimental results clearly confirm that the low fluorescence polarization value was indeed attributed to the weak affinity between the short FAM-DNA fragement and $TiS_2$ nanosheet, and was not caused by incomplete adsorption of the fragments. On
55 the other hand, the significant enhancement of the $\Delta FP$ value was attributed to the fact that $TiS_2$ could greatly enhance the background FP value and the $Zn^{2+}$ could catalyze the cleavage of DNAzyme complex formed from FR binding to probe 1 + probe 2 to achieve the target-recycling signal amplification.
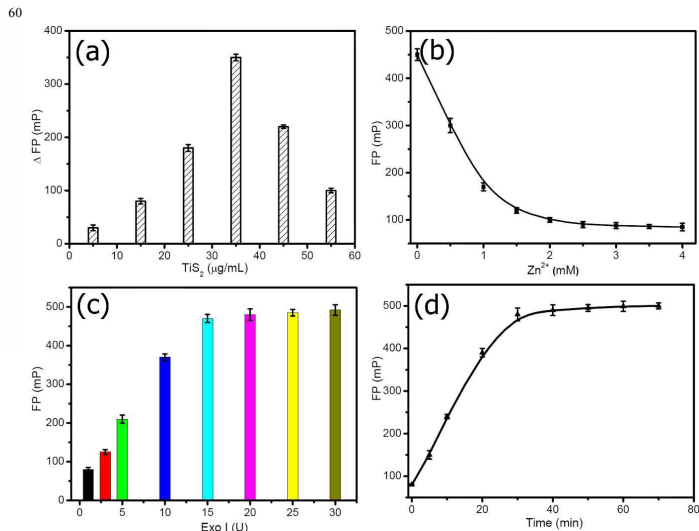
60



**Fig. 4** (a) The effect of $TiS_2$ concentration on the fluorescence polarization response of the sensing system, $\Delta FP = FP_0$-FP,
65 where $FP_0$ and $FP$ are the fluorescence polarization in the absence and presence of FR, respectively. [probe 1] = 48 nM, [probe 2] = 40 nM, [FR] = 5 ng/mL, $[Zn^{2+}]$ = 2 mM and [Exo I] = 10 U; (b) the effect of $Zn^{2+}$ concentration on the fluorescence polarization response of the sensing system. [probe 1] = 48 nM,
70 [probe 2] = 40 nM, [FR] = 5 ng/mL, $[TiS_2]$ = 35 µg/mL and [Exo I] = 10 U; (c) the effect of Exo I concentration on the fluorescence polarization response of the sensing system. [probe 1] = 48 nM, [probe 2] = 40 nM, $[TiS_2]$ = 35 µg/mL, $[Zn^{2+}]$ = 2.5 mM; (d) fluorescence polarization intensity of the sensing system
75 as a functiom of reaction time between probe 1 and Exo I. [probe 1] = 48 nM, [probe 2] = 40 nM, $[TiS_2]$ = 35 µg/mL, [Exo I] = 15 U, $[Zn^{2+}]$ = 2.5 mM.

In order to achieve the best assay performance, we optimized
80 the amplification sensing conditions for the detection of targets. It was fond that $TiS_2$ concentration was one of the critical factors in the detection system. When $TiS_2$ concentration was too low, the background FP value was rather low, possibly due to the incomplete adsorption of FAM-labeled probe 2 on $TiS_2$ surface.
85 However, when $TiS_2$ concentration was too high, the short FAM-linked DNA fragment released from DNAzyme hydrolyzing reaction could also be adsorbed on the excessive amount of $TiS_2$ nanosheets, resulting in a low change of $\Delta FP$ value. Thus, it is necessary to optimize the amount of $TiS_2$ to obtain the highest
90 $\Delta FP$ values. As shown in Fig. 4a, $\Delta FP$ value of the sensing

system increased significantly when the concentration of $TiS_2$ was increased from 0 to 35 μg/mL, then, it decreased with a further increase of $TiS_2$ concentration, which might be ascribed to the excessive adsorption effect of $TiS_2$ at a high concentration on the cleavage-produced short FAM-DNA fragments. Therefore, 35 μg/mL $TiS_2$ was chosen as the optimal concentration in the next experiments.

It was also found that the amount of $Zn^{2+}$ could influence the sensitivity of aptasensor. Thus, the effect of $Zn^{2+}$ concentration was studied and the results were shown in Fig. 4b. It is clear that the FP value of the sensing system decreased with increasing $Zn^{2+}$ concentration up to 2.5 mM. When the concentration was higher than 2.5 mM, the FP value of the sensing system reached a platform. Taking into account the response sensitivity, 2.5 mM of $Zn^{2+}$ was used in the final solution.

The concentration of Exo I and reaction time of Exo I-catalyzed digestion were also optimized by measuring the FP value of probe 2 as a function of reaction time. As shown in Fig. 4c, the FP value of FAM-labeled probe 2 increased sharply as the concentration of Exo I was increased from 0 to 35 U. When the concentration of Exo I was up to 15 U, the FP value of FAM labeled probe 2 was similar to that of the background signal (probe 2/$TiS_2$ system without probe 1). This suggests that probe 1 was completely hydrolyzed. As a result, 15 U was taken as the optimized concentration for Exo I. Fig. 4d shows the reaction time dependence of FP values for the reaction between probe 1 and Exo I. It can be seen that the reaction could be completed in about 30 min at 37 ℃.
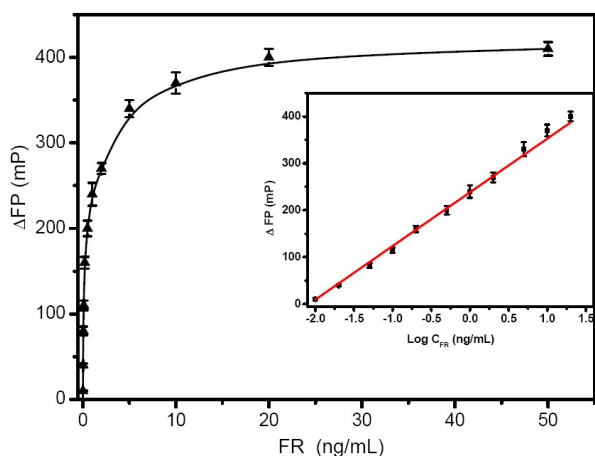


**Fig. 5** Fluorescence polarization change of the probe 1 + probe 2 + $TiS_2$ system incubated with different concentrations of FR in the presence of $Zn^{2+}$. The inset shows the linear relationship between $\varDelta FP$ values and FR concentrations. [probe 1] = 48 nM, [probe 2] = 40 nM, [$TiS_2$] = 35 μg/mL, [$Zn^{2+}$] = 2.5 mM, [Exo I] = 15 U). The error bar was calculated from three independent experiments.

Based on the above results, 35 μg/mL of $TiS_2$, 2.5 mM of $Zn^{2+}$, 15 U of Exo I and 30 min of reaction time were selected for the further detection experiments of FR. Under the optimal conditions, we investigated the $\varDelta FP$ values of the sensing system incubated with different concentrations of FR. As illustrated in Fig. 5, a dramatic increase in the $\varDelta FP$ value was observed with increasing concentrations of FR. By measuring the $\varDelta FP$ values of

the solution upon addition of different concentrations of FR, we obtained the working curve in the FR concentration range from 0.01 to 50 ng/mL. In the inset of Fig. 5, the $\varDelta FP$ values were found to increase monotonically with increasing concentration of FR, and showed a semi-logarithmic dependence on the FR concentrations over the range from 0.01 to 20 ng/mL. The correlation equation was $\varDelta FP = 238.3 + 114.3$ lg C (R=0.9969), where C is the concentration of FR. The detection limit was 0.003 ng/mL based on 3σ. A control experiment without $Zn^{2+}$ was carried out to confirm if the efficient $Zn^{2+}$-dependent DNAzyme-assisted target recycling signal amplification contributes to the high sensitivity of the approach. In doing so, probe 1 + probe 2 + $TiS_2$ system with different concentrations of FR was performed in the absence of $Zn^{2+}$. It can be seen from Fig. S5 that the limit of detection was 1.2 ng/mL. Thus, we can conclude that it is the $Zn^{2+}$-dependent DNAzyme-assisted target recycling signal amplification that lowers the limit of detection by three orders of magnitude for the detection of FR. In comparison with other DNA-based biosensors for FR (Table S2), $Zn^{2+}$-dependent DNAzyme-assisted target recycling sensor shows a lower detection limit than most of the previously reported DNA-based biosensors for FR.
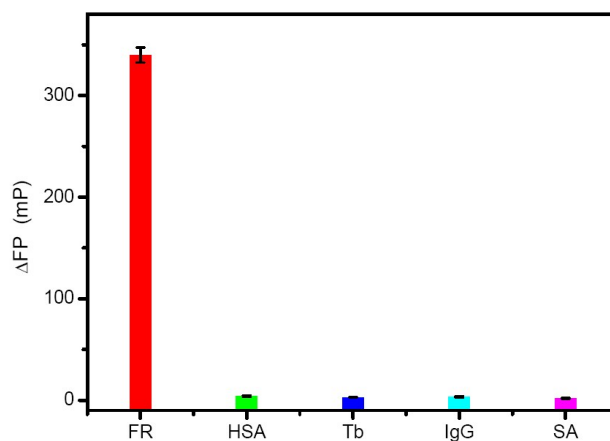


**Fig. 6** Selectivity of the sensing system for FR over other common biomolecules. The concentrations of biomolecules were: 5 ng/mL of FR, 5 μg/mL of human serum albumin (HSA), thrombin (Tb), immunoglobulin G (IgG) and streptavidin (SA), respectively. The error bar was calculated from three independent experiments.

To evaluate the specificity of the fabricated biosensor for FR, this sensor system was used for the detection of other biomolecules such as thrombin (Tb), human serum albumin (HSA), immunoglobulin G (IgG), and streptavidin (SA) under the same experimental conditions. As shown in Fig. 6, significant FP value enhancement was observed in the presence of FR, whereas the FP value remained quite low for the other tested analytes compared to the blank control sample even though their concentrations were 1000 times higher than FR. These results demonstrate excellent selectivity of the assay for FR, probably resulted from the specific and high affinity binding of FR to folate.

Considering the significance of FR analysis in biological

samples, the serum samples from three advanced ovarian cancer patients and three healthy women were used to evaluate the applicability of this approach. We investigated the level of FR in the above six serum samples by using our designed approach and
5 the validated commercial Folate Receptor 1 ELISA kit (Elabscience Biotechnology Co., Ltd. Wuhan, China), respectively. The detection results were presented in Table S3. It is clear that the results obtained from the approach designed in this work are in excellent agreement with those obtained by using
10 the commercial Folate Receptor 1 ELISA kit method. This suggests that our sensing system can potentially be applied for the detection of biological samples.

To examine if our signal amplification strategy can be applied to the detection of other molecules, we further designed $Zn^{2+}$-
15 dependent DNAzyme-assisted target recycling signal amplification method for the detection of thrombin (Tb) based on the terminal protection of biomolecules bound aptamer DNA. Scheme 2 illustrates the working mechanism of this homogeneous assay. At the 3'-terminus of probe 3, there is an
20 extend aptamer DNA sequence (green part) which can specifically bind Tb to form Tb/aptamer complex, and the rest of the sequence (red part) is the enzyme strand. In the absence of Tb, probe 3 can be hydrolyzed by Exo I from its 3'-terminus. With the introduction of Tb, the Tb/aptamer complex is able to protect
25 probe 3 from the Exo I digestion.[17] Therefore the terminal-protected probe 3, whose amount is positive correlative with the amount of Tb, can hybrid with probe 2 to form a $Zn^{2+}$-depended-DNAzyme structure, thus trigger the amplification process.
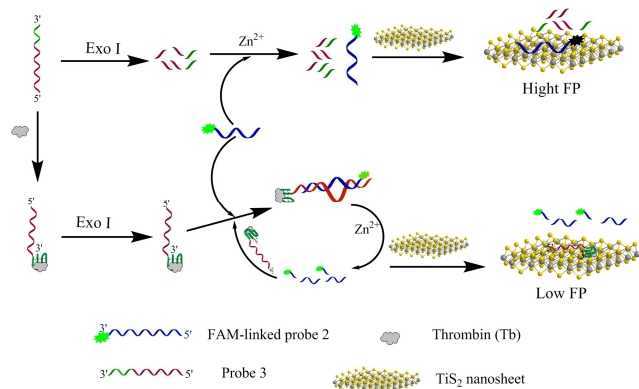
30 **Scheme 2** the working principle of $TiS_2$ nanosheet enhanced fluorescence polarization biosensor for thrombin detection via terminal protection of biomolecules bound aptamer DNA and DNAzyme-assisted signal amplification.

35

Similarly, the assay conditions were optimized to obtain the best performance of the sensing system. It was shown that using 25 μg/mL of $TiS_2$, 0.2 mM of $Zn^{2+}$ and 10 U of Exo I with incubation time of 50 min for enzyme hydrolysis reaction could
40 provide the maximum S/N ratio for the sensing system (see ESI, Fig. S6-9). Fig. 7 exhibits the changes in fluorescence polarization value upon addition of different concentrations of Tb, and a good linear relationship was observed between the *ΔFP* values and the Log $C_{Tb}$ over the range of 0.05 pM-100 nM (R =
45 0.9976). A detection limit of 0.01 pM was estimated for Tb based on 3σ. This detection limit is also about three orders of magnitude higher than that of the traditional homogeneous aptasensors, and

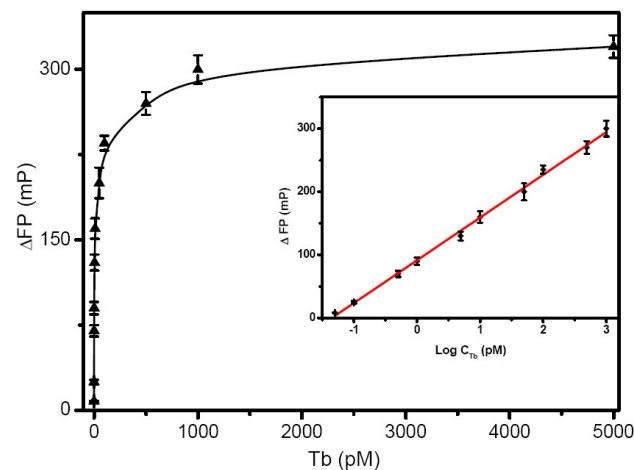is comparable to or better than that of the other reported amplified aptasensors (Table S4).

50 **Fig. 7** Fluorescence polarization changes of the probe 3 + probe 2 + $TiS_2$ system incubated with different concentrations of Tb in the presence of $Zn^{2+}$. The inset shows the linear relationship between the *ΔFP* values and the concentrations of Tb. [probe 3] =
55 30 nM, [probe 2] = 25 nM, [$TiS_2$] = 25 μg/mL, [$Zn^{2+}$] = 2.0 mM, [Exo I] = 10 U. The error bar was calculated from three independent experiments.

To test the specificity of the assay for Tb detection, we selected
60 four common biomolecules in the human blood (IgG, IgE, HSA and ATP) to perform the control experiments. As shown in Fig. S10, among these analytes, only Tb resulted in a significant increase in the ΔFP value, while the control molecules did not lead to any discernible FP value change, which indicates that our
65 sensing system exhibits an excellent selectivity to Tb over other competing analytes.

To examine the feasibility of our approach in complex biological matrixes, the determination of Tb in three healthy human plasma samples were performed. It can be seen from
70 Table 1 that the detection results of Tb in human plasma samples by the amplified aptasensor are in good agreement with those obtained by commercial ELISA kit method. Once again, it is comfirmed that the sensing approach developed in the present work can be applied for the detection of Tb in real biological
75 samples.

**Table 1.** Comparisons of the amplified approach developed in this work with the traditional ELISA kit method for the detection of Tb in the plasma samples.

80

| Sample | This work (μM)[a] | RSD (%, n=3) | ELISA (μM)[a] | RSD (%, n=3) |
|--------|-------------------|--------------|---------------|--------------|
| 1 | 20.63 | 2.5 | 20.40 | 2.6 |
| 2 | 28.35 | 2.8 | 28.45 | 3.6 |
| 3 | 35.48 | 2.4 | 35.53 | 3.0 |

[a] Each sample was analyzed in triplicate, and the results were the average values

## Conclusions

In summary, we report for the first time that transition metal dichalcogenides nanosheets (such as $TiS_2$ nanosheets) exhibit
differential affinity toward short oligonucleotide fragments versus ssDNA probes and can act as an efficient fluorescence polarization enhancer for the adsorbed fluorescence DNA probes. On the basis of this finding, we have developed a general fluorescence polarization method based on $TiS_2$ nanosheet, $Zn^{2+}$-
dependent DNAzyme-assisted signal amplification and terminal protection of single strand DNA for highly efficient detection of biomolecules, such as FR and Tb. This approach shows advantages such as high sensitivity, excellent specificity and simplicity. Combining the $TiS_2$ nanosheet enhanced back-ground
fluorescence polarization signal and $Zn^{2+}$- dependent DNAzyme-assisted signal amplification, the developed strategy has a detection limit of 0.003 ng/mL and 0.01 pM for FR and Tb, respectively, which are much lower than the most previously reported fluorescence biosensors. By taking advantage of the
highly binding specifics between DNA and targets, the developed biosensors show significantly high selectivity toward target (FR or Tb) and can distinguish the target biological small molecules from their analogues. Furthermore, the proposed method has been applied for the determination of FR and Tb in human serum with
satisfactory results, which suggests that these methods have great potential for diagnostic purpose. Therefore, it is expected that by designing the particular structure at the 3' terminal of the DNA probe, this simple and highly sensitive strategy would have important applications in a wide range of areas, such as biological,
medical diagnostics and environmental monitoring.

## Acknowledgements

## Notes and references

*a* *School of Environment, Henan Key Laboratory for Environmental Pollution Control, Key Laboratory for Yellow River and Huai River Water Environment and Pollution Control, Ministry of Education, Henan Normal University, Xinxiang, Henan 453007, P. R. China*

*b* *Department of Chemistry, Sanquan Medical College, Xinxiang Medical University, Xinxiang, Henan 453003 , P. R. China*

*c Life Science College, Henan Normal University, Xinxiang, Henan, 453007, P. R. China*

*\*Address correspondence to Jing Fan, School of Environment, Henan Normal University, Xinxiang, Henan 453007, P. R. China. Tel: +86-373-3325719. E-mail: fanjing@htu.cn*

† Electronic Supplementary Information (ESI) available: [Table S1-S4, Scheme S1, Figure S1-S10]. See DOI: 10.1039/b000000x/

1 (a) A. B. Chinen, C. M. Guan, J. R. Ferrer, S. N. Barnaby, T. J. Merkel, and C. A. Mirkin, *Chem. Rev.*, **2015**, *115*, 10530-10574; (b) E. Hendry, T. Carpy, J. Johnston, M. Popland, R. V. Mikhaylovskiy, A. J. Lapthorn, S. M. Kelly, L. D. Barron, N. Gadegaard and M. Kadodwala, *Nat. Nanotechnol.,* **2010,** *5,* 783-787; (c) H. Q. Zhang, F. Li, B. Dever, X. F. Li, and X. C. Le, *Chem. Rev.,* **2013**, *113*, pp 2812-2841.

2 (a) B. R. Stockwell, *Nat. Rev. Genet.*, **2000**, 1, 116–125; (b) Z. Wu, Z. Zhen, J. H. Jiang, G. L. Shen, R. Q. Yu, *J. Am. Chem. Soc.,* **2009,** 131, 12325-12332; (c) Z. Wu, H. Q. Wang, M. Guo, L. J. Tang, R. Q. Yu, J. H. Jiang, *Anal. Chem.,* **2011,** 83, 3104-3111; (d) X. L. Wang, F. Li, Y. H. Su, X. Sun, X. B. Li, H. J. Schluesener, F. Tang, S. Q. Xu, *Anal. Chem.,* **2004,** 76, 5605-5610; (e) D. M. Zheng, R. X. Zou, X. H. Lou, *Anal. Chem.*, **2012,** 84, 3554-3560.

3 (a) X. J. Yang, Z. Q. Gao, *Nanoscale*, **2014,** 6, 3055-3058; (b) G. F. Wang, X. P. He, L. Wang, X. J. Zhang, *Biosens. Bioelectron.,* **2013,** 42, 337-341; (c) Y. He, X. J. Xing, H. W. Tang, D. W. Pang, *small* **2013,** 9, 12, 2097-2101; (d) J. Zhao, S. S. Hu , Y. Cao, B. Zhang, G. X. Li, *Biosens. Bioelectron.,* **2015,** 66, 327-331; (e) B. Y. Jiang, M. Wang, C. Li, J. Q. Xie, *Biosens. Bioelectron.,* **2013,** 43, 289-292

4 (a) J. Ruta, S. Perrier, C. Ravelet, J. Fize, E. Peyrin, *Anal. Chem.* **2009,** 81, 7468-7473; (b) B. Yang, X. B. Zhang, L. P. Kang, G. L. Shen, R. Q. Yu, W. H. Tan, *Anal. Chem.,* **2013,** 85, 11518-11523; (c) D. P. Zhang, M. L. Lu, H. L. Wang, *J. Am. Chem. Soc.* **2011,** 133, 9188–9191; (d) D. M. Jameson, J. A. Ross, *Chem. Rev.* **2010,** 110, 2685-2708; (e) T. Jia, C. Y. Fu, C. S. Huang, H. T. Yang, N. Q. Jia, *ACS Appl. Mater. Interfaces,* **2015,** 7, 10013-10021.

5 (a) L. Cui, Y. Zou, N. H. Lin, Z. Zhu, G. Jenkins, C. Y. Yang, *Anal. Chem.,* **2012,** 84, 5535-5541; (b) Y. Huang, S. L. Zhao, Z. F. Chen, M. Shi, H. Liang, *Chem. Commun.,* **2012,** 48, 7480-7482; (c) Z. Y. Zhu, C. Ravelet, S. Perrier, V. Guieu, E. Fiore, E. Peyrin, *Anal. Chem.,* **2012**, 84, 7203-7211; (d) Y. Yu, Y. Liu, S. J, Zhen, C. Z. Huang, *Chem. Commun.,* **2013,** 49, 1942-1944; (e) X.Y. Wang, M. J. Zou, H. D. Huang, Y. Q. Ren, L. M. Li, X. D. Yang, N. Li, *Biosens. Bioelectron.,* **2013,** 41, 569-575; (f) B. C. Ye, B. C. Yin, *Angew. Chem. Int. Ed.,* **2008,** 47, 8386-8389; (g) Y. Huang, K. Hu, S. L. Zhao, M. Li, Z. F. Chen, Q. J. Lv, H. Liang, *Chem. Asian J.* **2014,** 9, 87-92.

6 (a) M. M Yan, W. H. Bai, C. Zhu, Y. F. Huang, J. Yan, A. L. Chen, *Biosens. Bioelectron.,* **2016,** 77, 613-623; (b) X. J. Xie, W. Xu, X. G. Liu, *Accounts. Chem. Res.,* **2012,** 45, 1511-1520; (c) C. Chen, C. Q. Zhao, X. Y. Yang, J. S. Ren, X. G. Qu, *Adv. Mater.,* **2010,** 22, 389-393.

7 (a) M. Zhang, Y. M. Guan, B. C. Ye, *Chem. Commun.,* **2011,** 47, 3478-3480, (b) J. J. Zhao, Y. F. Ma, R. M. Kong, L. L. Zhang, W. Yang, S. L. Zhao, *Analy. Chim. Acta.,* **2015**, 887, 216-223; (c) Y. Huang, X. Q. Liu, L. L. Zhang, K. Hu, S. L. Zhao, B. Z. Fang, Z. F. Chen, H. Liang, *Biosens. Bioelectron.,* **2015,** 63, 178-184; (d) Y. Huang, X. Q. Liu, H. K. Huang, J. Qin, L. L. Zhang, S. L. Zhao, Z. F. Chen, H. Liang, *Anal. Chem.,* **2015,** 87, 8107-8114.

8 (a) H. K. Kim, J. W. Liu, J. Li, N. Nagraj, M. X. Li, C. M. B. Pavot, Y. Lu, *J. Am. Chem. Soc.,* **2007,** 129, 6896-6902; (b) X. B. Zhang, Z. D. Wang, H. Xing, Y. Xiang, Y. Lu, *Anal. Chem.,* **2010,** 82, 5005-5011.

9 (a) S. F. Liu, C. B. Cheng, T. Liu, Li. Wang, H. W. Gong, F. Li, *Biosens. Bioelectron.,* **2015,** 63, 99-104; (b) X. H. Zhao, L. Gong, X. B. Zhang, B. Yang, T. Fu, R. Hu, W. H. Tan, R. Q. Yu, *Anal. Chem.,* **2013,** 85, 3614-3620.

10 H. Z. Gu, K. Furukawa, Z. Weinberg, D. F. Berenson, R. R. Breaker, *J. Am. Chem. Soc.,* **2013,** 135, 9121-9129.

11 (a) H. Zhang, *ACS NANO,* **2015,** 9, 9451-9469; (b) Y. Chen, C. L. Tan, H. Zhang, L. Z. Wang, *Chem. Soc. Rev.,* **2015,** 44, 2681-2701; (c) G. H. Yang, C. Z. Zhu, D. Du, J. J. Zhu, Y. H. Lin, *Nanoscale,* **2015,** 7, 14217-14231; (d) C. L. Tan, P. Yu, Y. L. Hu, J. Z. Chen, Y. Huang, Y. Q. Cai, Z. M. Luo, B. Li, Q. P. Lu, L. H. Wang, Z. Liu, H. Zhang, *J. Am. Chem. Soc.,* **2015,** 137, 10430-10436; (e) M. Wu, R. Kempaiah, P. J. Huang, V. Maheshwari, J. W. Liu, *Langmuir* **2011,** 27, 2731-2738; (f) Q. Xi, D. M. Zhou, Y. Y. Kan, J. Ge, Z. K. Wu, R. Q. Yu, J. H. Jiang, *Anal. Chem.,* **2014,** 86, 1361-1365.

12 Y. Zhang, B. Zheng, C. F. Zhu , X. Zhang, C. L. Tan , H. Li, B. Chen , J. Yang, J. Z. Chen, Y. Huang, L. H. Wang, H. Zhang, *Adv. Mater.,* **2015,** 27, 935-939

13 (a) C. W. Lin, X. J. Zhu, J. Feng, C. Z. Wu, S. L. Hu, J. Peng, Y. Q. Guo, L. L. Peng, J. Y. Zhao, J. L. Huang, J. L. Yang, Y. Xie, *J. Am. Chem. Soc.,* **2013,** 135, 5144-5151; (b) L. H. Yuwen, H. Yu, X. R. Yang, J. J. Zhou, Q. Zhang, Y. Q. Zhang, Z. M. Luo, S. Su, L. H. Wang, *Chem. Commun.,* **2016,** 52, 529-532

14 (a) X. Chen, H. L. Liu, X. D. Zhou, J. M. Hu, *Nanoscale* **2010,** 2, 2841-2846; (b) Y. H. Wang, L. Bao, Z. H. Liu, D. W. Pang, *Anal. Chem.,* **2011,** 83, 8130-8137.

15 (a) W. A.Henne, D. D. Doorneweerd, J. Lee, P. S. Low, C. Savran, *Anal. Chem.* **2006,** 78, 4880-4884; (b) A. Puig-Kroger, E. Sierra-Filardi, A. Dominguez-Soto, R. Samaniego, M. T. Corcuera, F. Gomez-Aguado, M. Ratnam, P. Sanchez-Mateos, A. L. Corbi, *Cancer Res.,* **2009,** 69, 9395-9403. (c) E. Basal1, G. Z. Eghbali-Fatourechi, K. R. Kalli, L. C. Hartmann, K. M. Goodman, E. L. Goode, B. A. Kamen, P. S. Low, K. L. Knutson, *PLoS ONE*, **2009**, 4, e6292.

16 M. Endo, Y. Takeuchi, Y. Suzuki, T. Emura, K. Hidaka, F. Wang, I. Willner, H. Sugiyama, *Angew. Chem.,* **2015,** 127, 10696-10700.

17 (a) X. L. Wang, F. Li, Y. H. Su, X. Sun, X. B. Li, H. J. Schluesener, F. Tang, S. Q. Xu, *Anal. Chem.,* **2004,** 76, 5605-5610; (b) D. M. Zheng, R. X. Zou, X. H. Lou, *Anal. Chem.,* **2012,** 84, 3554-3560; (c) Q. W, Xue, G. Zhang, L. Wang, W. Jiang, *Analyst,* **2014,** 139, 3167-3173.